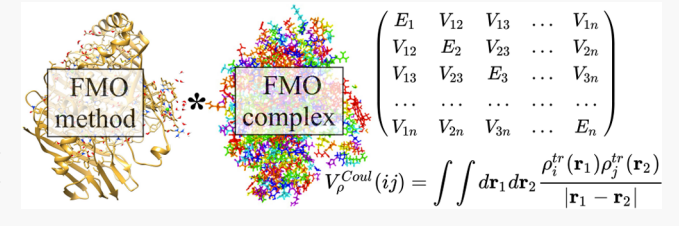


# FMOxFMO: Elucidating Excitonic Interactions in the Fenna-Matthews-Olson Complex with the Fragment Molecular Orbital Method

Danil S. Kaliakin, hiroya Nakata, Yongbin Kim, Qifeng Chen, Dmitri G. Fedorov, and Lyudmila V. Slipchenko\*,†

Supporting Information

ABSTRACT: In order to study Förster resonance energy transfer (FRET), the fragment molecular orbital (FMO) method is extended to compute electronic couplings between local excitations via the excited state transition density model, enabling efficient calculations of nonlocal excitations in a large molecular system and overcoming the previous limitation of being able to compute only local excitations. The results of these simple but accurate models are validated against full



quantum calculations without fragmentation. The developed method is applied to a very important photosynthetic pigmentprotein complex, the Fenna-Matthews-Olson complex (FMOc), that is responsible for the energy transfer from a chlorosome to the reaction center in the green sulfur bacteria. Absorption and circular dichroism spectra of FMOc are simulated, and the role of the molecular environment on the excitations is revealed.

# I. INTRODUCTION

Investigation of detailed mechanisms of energy transfer in pigment-protein complexes (PPC) provides knowledge necessary for the development of biomimetic systems such as bioinspired artificial antennas, light-harvesting materials, and artificial photosynthetic devices. 1-5 The object of the present study is the Fenna-Matthews-Olson complex, referred to as FMOc rather than FMO to distinguish it from the utilized computational technique, the Fragment Molecular Orbital method, which will be traditionally referred to as FMO. The FMOc is one of the most studied PPCs that over a few decades spawned a continuous interest from both experimental and theoretical groups. 6-15 The FMOc plays a crucial role in the photochemical apparatus of green sulfur bacteria transferring the excitation energy from the light-harvesting antennae (chlorosome) to the reaction center.

The FMOc consists of three identical monomers aligned in C<sub>3</sub> symmetry. The energy transfer within the FMOc occurs through bacteriochlorophyll a (BChl) molecules encapsulated within the protein matrix. Each monomer of the FMOc

experimental studies that BChl 3 is located near the reaction

ls among which six BChls are arranged in an vith BChl 7 being located in the middle of he eighth BChl is positioned between d is weakly bound to the protein surface, uent losses of this pigment during isolation of the protein. 18 It is known from center, 19-21 while BChl 1 and BChl 8 are in the closest proximity to the chlorosome.<sup>22</sup> Despite minor structural differences between the FMOc obtained from different species of green sulfur bacteria, all of them preserve similar optical signatures as well as the C<sub>3</sub> arrangement of monomers in the

While FMOc is one of the most studied PPCs, its excitonic interactions are still not entirely understood, and there is no consensus on the direction of energy transfer between BChls. 18,23 BChl 3 is commonly accepted as the exit point of photons from the FMOc into the reaction center.<sup>24</sup> However, there is no agreement on the photon entrance point from the chlorosome to the FMOc. Despite the fact the some of the studies suggest that the BChl 8 of the neighboring monomer could be an entrance point for the energy transfer from chlorosome, <sup>22,25</sup> the energetic properties of BChl 1 and BChl 6 also indicate that they are likely candidates for the role of the entrance point, which makes the indication of even initial energy transfer points debatable, let alone a whole map of energy transfer. <sup>26,27</sup>

Dynamics of electronic excitations in PPC and related photoactive materials such as biomimetic devices and artificial photosynthetic complexes is governed by the Förster resonance energy transfer (FRET). FRET has broad

Received: June 20, 2019 Published: December 16, 2019



pdfelement

Department of Chemistry, Purdue University, 560 Oval Drive, West Lafayette, Indiana 47907, United States

<sup>&</sup>lt;sup>‡</sup>Research Institute for Advanced Materials and Devices, Kyocera, 5-3 Hikaridai-3, Seika-cho Soraku-gun, Kyoto 619-0237, Japan

<sup>§</sup>Research Center for Computational Design of Advanced Functional Materials (CD-FMat), National Institute of Advanced Industrial Science and Technology (AIST), Central 2, Umezono 1-1-1, Tsukuba 305-8568, Japan

applications in biology, chemistry, and materials science as a tool to measure changes in distances between molecular domains such as a protein, a cellular structure, or a nanoparticle.<sup>28–36</sup> Modeling of resonance energy transfer requires information about excitation energies and electronic couplings between interacting pigments, which constitute the electronic Hamiltonian, as well as information about interactions of pigments' electronic degrees of freedom with bath, i.e., vibrational levels of pigments and protein scaffold. Eigenvalues and eigenvectors of the electronic Hamiltonian are the main components determining shapes of absorption and circular dichroism (CD) spectra. However, it is challenging to obtain realistic distribution of site energies from the firstprinciples calculations without fitting parameters. 23,25,27,38-44 The challenge to reproduce experimental spectra of FMOc by computational methods might be due to several reasons, including inadequate sampling of protein conforma-tions, <sup>23,27,40,45</sup> approximations undertaken for describing electronic structure and couplings between BChls, and interactions between BChls and the protein environment.<sup>46</sup>

In this work we introduce a new computational chemistry model based on the FMO-TDDFT method 47,48 that is capable of describing delocalized excitonic interactions in multichromophore systems such as pigment-protein complexes. While the FMO method is an all-electron fragmentation technique, the introduced model allows calculations of delocalized electronic excitations, which expands the FMO method to a new range of applications in molecular crystals and photosynthetic complexes. Here we utilize the developed model to demonstrate that the quantum-mechanical description of a protein environment makes a noticeable difference in excitation energies and electronic couplings in the FMOc pigment-protein complex. For this, we compare the excitation energies of FMOc calculated with the FMO method to those obtained from the quantum mechanics/molecular mechanics (QM/MM) model. We also elucidate the difference between the electronic couplings of BChls calculated with two different approximations, namely using transition dipoles or transition densities of each BChl pigment. Obtained data suggest that the theoretical absorption and CD spectra of FMOc are strongly affected by the description of the protein environment and to a lesser degree by a choice of the approximation utilized for computing electronic couplings between BChls.

# **II. THEORETICAL DETAILS**

The energy transfer in multichromophore systems occurs through two distinct types of interactions between pigments, namely long-range Coulombic interactions and charge-transfer mediated short-range interactions 8,46,49–53

$$V^{Elec} = V^{Coul} + V^{Short} \tag{1}$$

where  $V^{Elec}$  is the total electronic coupling,  $V^{Coul}$  is the Coulomb interaction between electronic transitions, and  $V^{Short}$  is the short-range electronic coupling that depends on intermolecular orbital overlap. The later term in eq 1 arises

p of molecular orbitals in interacting a can be further classified by exchange, e-transfer contributions.<sup>8,54</sup> However, since conentially with the distance between is negligibly small for pigments that are ntact<sup>8,56,57</sup> and typically does not contribute

significantly to the excitation energy transfer in the case of bright singlet excitations. Under this assumption the electronic interactions between pigments can be approximated with the Coulomb coupling term expressed using transition densities of the pigments as

$$V_{\rho}^{Coul}(ij) = \iint d\mathbf{r}_1 d\mathbf{r}_2 \frac{\rho_i^{tr}(\mathbf{r}_1)\rho_j^{tr}(\mathbf{r}_2)}{|\mathbf{r}_1 - \mathbf{r}_2|}$$
(2)

where  $\rho_i^{tr}$  and  $\rho_j^{tr}$  are the transition densities of the pigments i and j, respectively, defined as

$$\rho^{tr}(\mathbf{r}) = N \int \dots \int \Psi_{ex}^{*}(\mathbf{r}, \mathbf{r}_{2}, \dots, \mathbf{r}_{N}) \Psi_{gr}(\mathbf{r}, \mathbf{r}_{2}, \dots, \mathbf{r}_{N}) d\mathbf{r}_{2} \dots d\mathbf{r}_{N}$$
(3)

Here  $\Psi_{ex}$  and  $\Psi_{gr}$  are the wave functions of the excited and ground states of a pigment, respectively, and N is the number of electrons in this pigment.

By expanding transition densities in multipolar series and keeping only the leading dipole terms, the Coulomb coupling can be approximated as

$$V_{\mu}^{Coul}(ij) = \frac{\mu_i \mu_j}{R_{ij}^3} [\vec{\mu}_i \cdot \vec{\mu}_j - 3(\vec{\mu}_i \cdot \vec{n}_{ij})(\vec{\mu}_i \cdot \vec{n}_{ij})]$$
(4)

where  $\mu_i$  and  $\mu_i$  are the magnitudes and unit vectors of transition dipole moments for pigment i, respectively,  $R_{ij}$  is the distance between the transition dipoles, and  $n_{ij}$  is the corresponding direction. While the transition density approximation (eq. 2) offers accurate treatment of Coulomb couplings, <sup>27,46</sup> the transition dipole approximation provides a simple way to quickly estimate these couplings. Exact values of electronic couplings can be computed from dimer calculations, for example, using the fragment excitation density (FED) method. <sup>58</sup>

In the FED method the excited states calculations are performed on the entire (nonfragmented) system, while "fragments" define parts of the system that correspond to donor and acceptor. In this method the electronic coupling is expressed through electron (attachment) and hole (detachment) densities:

$$\rho_{elec}^{(mn)}(\mathbf{r}) = \sum_{ab}^{vir} \sum_{y}^{occ} a_{ya}^{(m)} a_{yb}^{(n)*} \psi_a(\mathbf{r}) \psi_b^*(\mathbf{r})$$
(5)

$$\rho_{hole}^{(mn)}(\mathbf{r}) = \sum_{yz}^{occ} \sum_{a}^{vir} a_{ya}^{(m)} a_{za}^{(n)*} \psi_{y}(\mathbf{r}) \psi_{z}^{*}(\mathbf{r})$$

$$(6)$$

In eqs 5 and 6,  $\psi$  denotes molecular orbitals, a represents excitation/de-excitation amplitudes, y/z are the indices of occupied orbitals of electronic states m and n, respectively, while a/b subscripts are the indices of virtual orbitals corresponding to these electronic states. Based on the electron and hole densities one can define the excitation density for electronic states m and n:

$$\rho_{ex}^{(mn)}(\mathbf{r}) \equiv \rho_{hole}^{(mn)}(\mathbf{r}) + \rho_{elec}^{(mn)}(\mathbf{r})$$
(7)

Using the excitation density, it is possible to express the excitation difference for electronic states m and n of donor i and acceptor j as

$$\Delta x_{mn} = \int_{\mathbf{r} \in i} \rho_{ex}^{(mn)}(\mathbf{r}) d\mathbf{r} - \int_{\mathbf{r} \in j} \rho_{ex}^{(mn)}(\mathbf{r}) d\mathbf{r}$$
(8)

where *i* and *j* could be space separated pigments or could be covalently bound donor and acceptor parts of the same molecule.

Based on eqs 5-8 one can define the electronic coupling within the FED approach as

$$V^{\text{FED}} = \frac{(E_m - E_n)|\Delta x_{mn}|}{\sqrt{(\Delta x_{mm} - \Delta x_{nn})^2 + 4\Delta x_{mn}^2}}$$
(9)

where  $E_n$  and  $E_m$  are the energies of the electronic states n and m, respectively. If pigments i and j are equivalent by symmetry,  $V^{\rm FED}$  becomes equal to one-half of the energy gap between states m and n. Despite being computationally more expensive (the excited state calculations are performed on a whole nonfragmented system), the FED approach provides a reliable reference for benchmark calculations of electronic couplings, being limited only by the accuracy of the chosen level of theory. The Q-Chem electronic structure package (version 5.0) offers FED calculations of electronic couplings based on the CIS, RPA, TD-DFT/TDA, and TD-DFT methods.  $^{59}$ 

The treatment of pigment protein systems with all-electronic methods is a challenging problem due to the size of these systems. The fragment molecular orbital (FMO) method is used to reduce computational cost, which enables all-electron treatment of the system using fragmentation. The FMO method is implemented in multiple quantum chemical packages, including ABINIT-MP, GAMESS, 2 PAICS, and OpenFMO. The FMO method has been used to compute nonlocal excitations using configuration interaction and as a supplementary tool. In this work the FMO method in GAMESS is used.

The FMO method in GAMESS has been interfaced with several quantum chemical models, including density functional theory (DFT),<sup>67</sup> multiconfigurational self-consistent field (MCSCF),<sup>68</sup> MP2 perturbation theory,<sup>69</sup> coupled cluster methods,<sup>70</sup> and time-dependent density functional theory (TD-DFT).<sup>67,71</sup> The method was proved to be highly scalable and has been efficiently parallelized and successfully run on over 160,000 CPU cores.<sup>72</sup> Moreover, the FMO method has been shown to be an efficient tool in studies of biological systems. Among many notable examples the most recent ones are the study of potent inhibitors for vitamin-D receptor,<sup>73</sup> the search of novel natural products for prion disease,<sup>63,74</sup> and the study of interaction between sarco/endoplasmic reticulum Ca<sup>2+</sup>-ATPase and its inhibitor thapsigargin toward antimalarial development,<sup>75</sup> as well as mapping interaction energies in chorismate mutase.<sup>76</sup>

The FMO method splits a molecular system into individual fragments and describes each fragment in a polarizable Coulomb bath of other fragments. The fragmentation of proteins is performed at  $C\alpha$ –C single bonds following peptide bonds. In FMO1, fragments polarized by the embedding potential are calculated. The accuracy can be improved in FMO2 through introducing dimer calculations that add charge

nge, where the total energy is calculated f electrostatically embedded monomers and p-body expansion.<sup>47</sup> Such treatment of the vs for explicit calculations of quantum tions within the dimer pairs. In principle, e improved by using three- and four-body

expansions (FMO3 and FMO4), but the comparative studies demonstrated that for the majority of applications the FMO2 is

sufficiently accurate. However, in this particular study we limited calculations to the FMO1 level of theory due to the large size of the pigment fragments.

Electronic excited states of pigments are computed using FMO1-TDDFT. 67,71 This formalism implies calculations of TDDFT excitation energies for selected fragments in the presence of the Coulomb field that is generated based on the self-consistently converged electronic densities of other fragments. 71,77 In this work we extended the capabilities of FMO-TDDFT to computing electronic couplings between chromophores. The procedure works in the following manner. First, after self-consistent convergence of electronic densities of all fragments, excitation energies and transition properties, including transition densities and transition dipole moments, are computed and stored for a selected subset of fragments. Second, computed transition densities and transition dipole moments are utilized for evaluation of electronic couplings either using eq 2 or eq 4. The computer code for computing electronic couplings in the FMO method is implemented in the GAMESS electronic structure package. 78,79

While FMO1-TDDFT describes the ground electronic state fully consistently with electronic densities of all fragments, which corresponds to a polarizable embedding model, the response of the polarizable environment to the density of an excited state is not directly accounted for. Thus, the FMO1-TDDFT model captures a zero-order effect of polarizable environment (which is often the leading contribution) through modification of occupied and virtual orbitals that are used to form the excited states during the TDDFT calculations. The present scheme neglects the dynamical response of the polarizable environment to the excitation energies and electronic couplings. These effects were investigated in a context of polarizable QM/MM and QM/PCM models. 80–85

Computed excitation energies and electronic couplings are combined in the electronic (excitonic) Hamiltonian, which is subsequently diagonalized for prediction of absorption and circular dichroism (CD) spectra. The CD optical activity is the result of the different indices of refraction for left and right plane-polarized light when it travels through the molecules, which results in different absorption of left- and right-handed circularly polarized light. This makes the CD spectroscopy especially useful in identification of intra- or intermolecular asymmetry of the molecular structures and, in the case of pigment—protein systems, provides information on relative orientation of pigments.

The general form of electronic Hamiltonian matrix  $H^{elec}$  for n interacting pigments in the system could be represented by the formula

$$H^{elec} = \begin{pmatrix} E_1 & V_{12} & V_{13} & \cdots & V_{1n} \\ V_{12} & E_2 & V_{23} & \cdots & V_{2n} \\ V_{13} & V_{23} & E_3 & \cdots & V_{3n} \\ \cdots & \cdots & \cdots & \cdots & \cdots \\ V_{1n} & V_{2n} & V_{3n} & \cdots & E_n \end{pmatrix}$$
(10)

where  $E_i$  is the excitation (site) energy of pigment i, and  $V_{ij}$  is the electronic couplings between pigments i and j. The diagonalization of this Hamiltonian provides the eigenvalues  $(\varepsilon)$  and eigenvectors (U) that could be used to model the absorption and circular dichroism (CD) spectra through computing oscillator  $(f_k)$  and rotary  $(r_k)$  strengths, respectively  $^{89,90}$ 

pdfelement

$$f_{k} = \sum_{i,j} (\overrightarrow{\mu_{i}} \cdot \overrightarrow{\mu_{j}}) U_{ik} U_{jk}$$

$$\tag{11}$$

$$r_k = \sum_{i,j} \varepsilon_k [\vec{R}_{ij}(\vec{\mu}_i \times \vec{\mu}_j)] U_{ik} U_{jk}$$
(12)

where i and j are the indices of chromophores, k is the index of the excitonic state,  $\mu_{i/i}^{\rightarrow}$  are the transition dipole moments for chromophores i or j, and  $\vec{R_{ii}}$  is the distance between the transition dipoles.

Generally, profiles of electronic absorption and CD spectra are affected by thermal motion of the system and interactions of electronic states of BChls with vibrational bath. Here we leave a detailed investigation of these effects for future work and focus on analysis of the influence of the protein environment on the electronic excitations and couplings. Thus, we convolute theoretical stick spectra for absorption and CD (eqs 11 and 12) with Gaussian functions 91 with full-width at half-maximum (fwhm) of 50 cm<sup>-1</sup>, which approximately corresponds to thermal broadening at 70 K.

#### III. COMPUTATIONAL DETAILS

The structure of the FMOc for quantum mechanics/molecular mechanics (QM/MM) and FMO simulations was obtained from a single representative snapshot from molecular dynamics (MD) trajectory of the solvated FMOc trimer. MD simulations were performed with the molecular modeling software AMBER (Version 14).92 The initial trimer structure of the FMOc was obtained from protein databank entrance 3ENI<sup>93</sup> and protonated using AMBER with correspondence to neutral pH. The system was solvated with 8893 water molecules and neutralized with six sodium ions for the total zero charge of the model (Figure 1a). The AMBER ff14SB<sup>94</sup> force field was used for simulating the protein chain, TIP3P95 for was used for describing water molecules, GAFF<sup>96</sup> was used for ions, and the AMBER-compatible force field defined specifically for BChl a chromophores<sup>97</sup> was employed. Initial NVT and NPT equilibrations were performed for 500 ps each, while an NPT production run was performed for 40 ns. The environmental conditions were defined as 300 K and 1 atm. The long-range interactions had a 10 Å cutoff; electrostatic interactions were treated with the particle mesh Ewald method. 98,99 Based on a randomly selected snapshot from the MD trajectory of the FMOc trimer, we created the FMOc monomer model by removing two other monomers and the majority of water molecules. The resulting model contained eight BChls as well as all amino acid residues and water molecules pertaining to the FMOc monomer unit, which resulted in 207 water molecules, eight BChl a molecules, 358 protein residues, and a total of 6853 atoms. Water molecules pertaining to the FMOc monomer were selected using an automated tool of UCSF Chimera<sup>100</sup> that allows for locating water molecules forming the solvation sphere around the given protein system. To investigate a sensitivity of the results to a specific protein structure, we repeated the procedure for four

elected snapshots keeping the consistent iter molecules in each conformer. Finally, mer model of conformer 1, we created the containing only BChl a molecules without acid residues (Figure 1b).

simulations of the monomer model were performed using full TDDFT (without imposing Tamm-Dancoff approximation) with the PBE0 functional, 101 the 6-

pdfelement

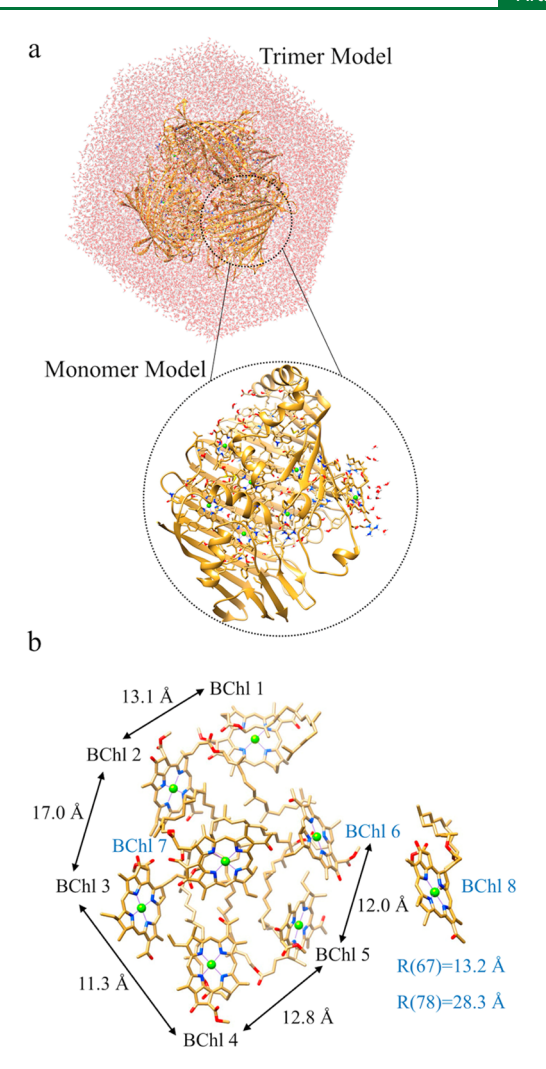


Figure 1. Models of the FMOc. a) Trimer and monomer models of the FMOc and b) the bare BChl model of the FMOc containing eight isolated BChl a molecules.

 $31G^*$  basis set,  $^{102}$  and electrostatic embedding with the same force fields as utilized in MD simulations. These simulations were performed with the QCHEM 5.0 quantum chemical package.<sup>59</sup> The choice of the functional was based on the previous study by List et al., 41 which shows that the PBE0 functional provides the most accurate excited state energies and transition dipoles of BChls in the FMOc among several functionals and wave function methods, compared to DFT-BHLYP/MRCI calculations. Quantum-mechanical regions in QM/MM calculations included single BChl a chromophores leading to eight distinct QM/MM setups. Each QM region included a phytol tail of BChl a but none of the surrounding protein residues.

The FMO simulations were performed with the GAMESS software package  $^{78,79}$  with the same basis set and the TDDFT functional as in the case of QM/MM calculations. Parameter RESPPC was set to two. The DFT and TDDFT calculations were performed with the SG1 grid. In order to achieve better convergence of self-consistent charge (SCC) during ground state FMO calculations, we combined pairs of negatively and positively charged residues located within 5 Å from each other into single fragments, which allowed for less charge transfer between fragments and more consistent electrostatic field. The list of negatively and positively charged fragments that are combined pairwise can be found in the Supporting Information. Residues coordinating Mg atoms of BChls were included in corresponding BChl fragments. In the case of BChl 5 two nearest residues were included to avoid fragmentation next to the carbonyl group that is in direct proximity to Mg atom. This resulted in the following combinations of fragments: HID103-BChl1, WAT2729-BChl2, HID290-BChl3, HID282-BChl4, LEU234-PHE235-BChl5, HID138-BChl6, HID103-BChl7, and TYR117-BChl8. Overall, this fragmentation scheme contained 405 fragments.

A series of benchmark calculations were also conducted on reduced-size model systems. To compare transition density and transition dipole models, we created a dimer model system, consisting of two identical BChl-like molecules with varying vertical and horizontal separations. Structures of these BChl-like molecules were prepared by isolating a central BChl (BChl 7) of the FMOc monomer, removing its phytol tail, and reoptimizing its geometry with the PBE0/6-31G\* level of theory. This model system is shown in Figure S2 of the Supporting Information. In order to investigate the influence of fragmentation of phytol tails on the FMO excitation energies and electronic couplings, we performed FMO calculations on a "bare" BChl model system (see Figure 1b) with phytol tails being included in BChl fragments (i.e., eight-fragment system) and with phytol tails being assigned as separate fragments (16fragment system). To resolve the importance of inclusion of Mg-coordinating residues into BChl fragments, we compared excitation energies from the two-fragment (BChl and residue) FMO calculations with conventional TDDFT excitation energies of nonfragmented systems. These calculations were performed on three model systems, HID103-BChl1, WAT2729-BChl2, and LEU234-PHE235-BChl5, which cover all three types of Mg-coordinating residues in the FMOc, namely coordination with nitrogen of a histidine, coordination with oxygen of a water molecule, and coordination with oxygen of a carbonyl group. The models utilized in these calculations are shown in Figure S3 of the Supporting Information.

#### IV. RESULTS AND DISCUSSION

pdfelement

A. Electronic Couplings with the FMO Method. The goal of this section is to validate a developed transition density approach within the FMO method and provide basic benchmarks of expected deviations of electronic couplings computed with transition density and transition dipole models at interpigment separations characteristic for the FMOc. Figure 2 compares electronic couplings computed using transition dipoles (eq 4) and transition densities (eq 2) within the FMO method, as well as using full-dimer calculations with the FED method (eq 9). The couplings are computed at different vertical displacements between two BChl molecules with stripped-off phytol tails (see the Computational Details section). Calculations are performed at the TDDFT PBE0/6-31G\* level of theory.

Analysis of data shown in Figure 2 suggests that the transition dipole approximation in the FMO method closely

and line, showing that a mutual polarization ered distances does not affect excited state institution density approximation deviates by m the exact electronic coupling (FED) data ations, respectively. However, at separations ant for the FMOc, namely 12–18 Å, these

deviations do not exceed 10 cm<sup>-1</sup>, which suggests that the exchange and overlap contributions can be neglected in

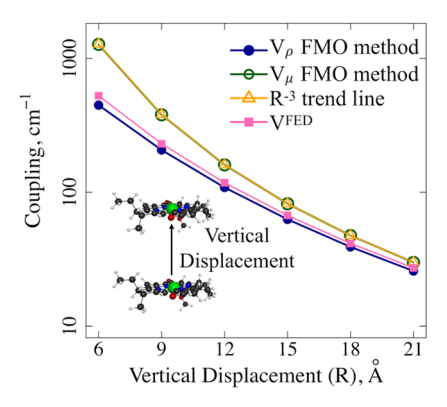
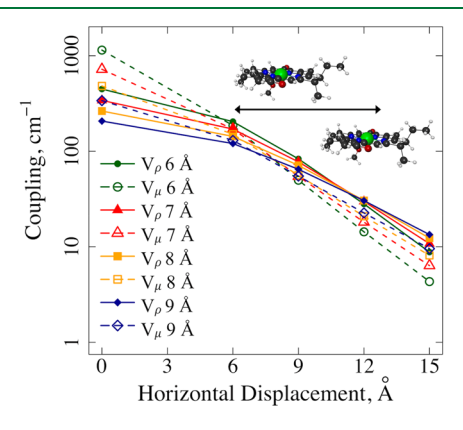


Figure 2. Electronic couplings computed with the transition dipole  $(V_{\mu})$  and transition density  $(V_{\rho})$  approximations within the FMO formalism and with the FED method  $(V^{\text{FED}})$ , as a function of vertical displacement between two stripped BChl molecules. The  $R^{-3}$  trend line shows a close agreement of the transition dipole approximation in the FMO formalism to the asymptotic behavior expected from eq 4.

calculations of couplings between BChls of the FMOc. On the other hand, it is clearly seen that the transition dipole approximation deviates significantly from the transition density model and exact coupling. The discrepancy between transition density and transition dipole approximations at 6 Å separation is 828 cm<sup>-1</sup> or 65%, while at 12 Å it is still as high as 52 cm<sup>-1</sup> or 32%. These results are in agreement with previous studies<sup>55,58</sup> and highlight the limitations of transition dipole model.

Comparison of the transition density and transition dipole predictions for various horizontal displacements between BChls is shown in Figure 3. While for all vertical separations



**Figure 3.** Transition density  $(V_{\rho}$ , solid lines) and transition dipoles  $(V_{\mu}$ , dashed lines) couplings as the function of horizontal displacement for various vertical displacements between two stripped BChl molecules.

the coupling values decrease with increasing the horizontal displacement (i.e., couplings decrease with increasing the overall distance between chromophores), the decay of the coupling as a function of the horizontal displacement occurs faster at smaller vertical separations and slower at larger vertical separations. This trend is observed for both transition density and transition dipole models. Additionally, as seen in Figure 3, the transition dipole approximation overestimates the coupling values at small horizontal displacements (between 0 and 9 Å) but underestimates the coupling strength at larger horizontal displacements (9–15 Å). This trend is the same for different

vertical separations. Overall, the transition dipole approximation provides a larger span of the coupling values at considered interpigment separations, while the transition density model results in more uniform couplings.

# B. Electronic Couplings between BChls in the Bare BChl Model. The Effect of Fragmentation on Couplings.

There are two governing criteria for fragmentation in the FMO method, namely the computational efficiency and accuracy of calculations. The most computationally efficient fragmentation scheme is the one in which fragments are of the same size, i.e., contain an equal number of basis functions. 103 However, the introduction of additional fragmentation points often leads to the decrease of accuracy, especially for conjugated systems.<sup>47</sup> In the case of FMOc the substantial reduction in computational cost could be achieved through fragmentation of BChl a pigments into two individual fragments, namely bacteriochlorin and the phytol tail. In this fragmentation scheme the bacteriochlorin part of the pigment is treated with TDDFT, while the phytol tail is described with DFT as all other fragments. However, such a fragmentation scheme prevents propagation of transition density onto the phytol tail and could lead to inaccuracies in the excitation energies and electronic

To test the effect of tail fragmentation on the excitation energies and couplings, we utilized the bare BChl model (Figure 1b). The phytol tail fragmentation is represented in Figure S4a of the Supporting Information. The fragmentation schemes with the attached and detached phytol tails are depicted in Figure S4b of the Supporting Information. Comparisons between site energies and couplings with the fragmentations including and excluding phytol tails, i.e., containing 8 or 16 FMO fragments, respectively, are shown in Figures 4a and 4b. The electronic Hamiltonians obtained with the two fragmentation schemes are provided in Tables S1 and S2 of the Supporting Information.

As can be seen from Figure 4a, the tail fragmentation affects the site energies of BChl 1 and BChl 4 by 89 and 126 cm<sup>-1</sup>, respectively. The drastic effect of the tail on excitation energies in these particular BChls is consistent with the previous study. 40 The differences in the electronic couplings computed with two fragmentation schemes are not as pronounced as the differences in excitation energies (Figure 4b). The most significant difference in couplings is observed for a pair of BChl 3 and BChl 4 and does not exceed 15 cm<sup>-1</sup>. The effect on site energies by the choice of fragmentation scheme in the case of BChl 1 and 4 is the result of the configuration of phytol tails in these pigments. The phytol tails of BChl 1 and of BChl 4 are bent toward bacteriochlorin part of the pigment, such that the double C=C bond on the tail participates in the electronic excitation and accumulates some amount of transition density. The fragmentation of the tail prevents the propagation of the electronic density over the phytol tail and constrains the excitation to the bacteriochlorin part, resulting in nonnegligible changes in the site energies. The inclusion of phytol tails into bacteriochlorin head fragments of BChls 2, 3, 5, and



al for the accuracy of site energies as in the and 4 but is preferable for a consistency in bigments. The importance of inclusion of FDDFT region for BChls 1 and 4 is further ct that the Hamiltonians produced with two mes result in noticeably different absorption

and CD spectra as demonstrated in Figure S5 of the Supporting Information.

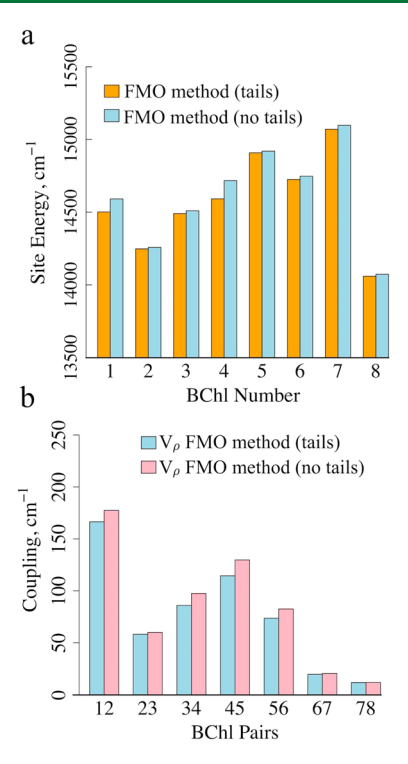


Figure 4. (a) Excitation energies and (b) electronic couplings in the bare BChl model obtained with two FMO method fragmentation schemes. The "tails" label indicates the fragmentation scheme in which phytol tails are included in the BChl fragments (with a total of 8 FMO fragments), while "no tails" marks the fragmentation scheme in which the phytol tails are separated as individual fragments (with a total of 16 FMO fragments).

The next important question is the effect of inclusion of neighboring amino acid (AA) residues into BChl fragments. The reasoning here is the same as in the case of the phytol tail exclusion/inclusion, i.e., the search for optimal balance between the computational efficiency and the accuracy of calculations. The most significant influence on excitation energies is expected from the residues coordinating Mg atoms of BChls. Accordingly, we consider three representative model systems, BChl 1 coordinated with N atom of histidine, BChl 2 coordinated with a water molecule, and BChl 5 coordinated with a carbonyl group (see Figure S3). These three models cover all types of Mg-coordinating residues in the FMOc. The excitation energies are calculated using conventional TDDFT  $(E_{\text{TDDFT}})$  on the dimer and the FMO method  $(E_{\text{FMO}})$  with the fragmentation in which the Mg-coordinating residues are assigned as separate fragments. The resulting excitation energies and differences between them are shown in Table 1.

As could be seen from Table 1, the exclusion of nearest residues from the FMO-TDDFT calculations leads to inaccuracies in excitation energies as large as  $-210 \text{ cm}^{-1}$  in

Table 1. Excitation Energies in BChl-AA Pairs Computed with Two-Fragment FMO  $(E_{\rm FMO})$  and with TDDFT Calculations on the Dimer  $(E_{\rm TDDFT})$  and the Differences between Them  $(\Delta E = E_{\rm TDDFT} - E_{\rm FMO})$ 

| BChl | $E_{\rm FMO}$ , cm <sup>-1</sup> | $E_{\mathrm{TDDFT}}$ , cm <sup>-1</sup> | $\Delta E$ , cm <sup>-1</sup> |
|------|----------------------------------|---|-------------------------------|
| 1    | 14477.6                          | 14550.2                                 | 88.7                          |
| 2    | 14316.3                          | 14324.3                                 | 8.1                           |
| 5    | 14880.8                          | 14735.7                                 | -209.7                        |

the case of BChl 5 and 88.7 cm<sup>-1</sup> for BChl 1, which are nonnegligible for building accurate electronic Hamiltonian from the first principles. In order to understand the origin of errors in the excitation energies due to fragmentation of Mgcoordinating residues, we considered four parameters, namely bond lengths between Mg and N or O atoms of coordinating AA (Mg-AA) and binding energies, as well as changes in the magnitudes of transition dipole moments and transition densities between BChl-AA dimers and bare BChls. The Mg-AA bond lengths for BChls 1, 2, and 5 are 2.75, 2.57, and 3.07 Å, respectively, while the corresponding binding energies are 18.4, 17.0, and 13.9 kcal/mol. Thus, these two metrics do not correlate with the error in the FMO excitation energies upon fragmentation. On the other hand, differences in the magnitudes of the transition dipoles between fragmented and nonfragmented (fully quantum) BChl-AA pairs are 0.160, 0.005, and 0.219 D, for BChl 1, 2, and 5, respectively, which correlates well with the errors due to fragmentation. Similarly, analysis of transition densities for BChl1, BChl2, and BChl5 (Figure 5a, b, and c) demonstrates that while in all three cases

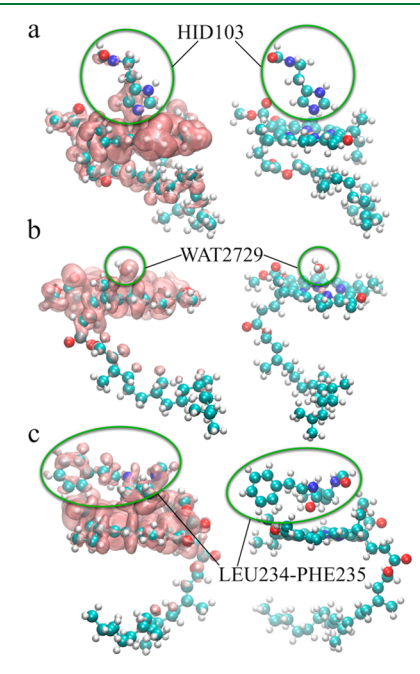


Figure 5. Transition densities of BChls with Mg-coordinating residues (left) and the molecular structures of these systems (right). a) BChl1-HID103, b) BChl2-WAT2729, and c) BChl5-LEU234-PHE235.

transition density "leaks" into Mg-coordinating fragments, the effect is more pronounced in the case of BChl5 and BChl1 and is smaller for BChl2. Therefore, we conclude that the largest FMO errors in excitation energies are associated with delocalization of an excited state into surrounding residues. These errors could be corrected by increasing the size of the

r by invoking two-body corrections for the The observed dependence of calculated site e of the TDDFT region is consistent with eviously published QM/PCM and QM/s by Jurinovich et al. where the inclusion of e TDDFT (QM) region in QM/PCM and

QM/MMpol calculations affected the excitation energies by 20 and 10 meV ( $\sim$ 160 and 80 cm<sup>-1</sup>), respectively.<sup>40</sup>

pdfelement

As could be seen from Figure 5a, the transition density of BChl1 has a significant portion on the phytol tail, which explains a high impact of the phytol tail fragmentation on the excitation energy of this particular pigment. Based on data presented in Figure 4, Figure 5, and Table 1, we conclude that it is essential to include both phytol tail and the Mg-coordinating residues in the BChl fragments in order to achieve quantitative accuracy in describing FMOc site energies and couplings with the FMO method.

D. Electronic Hamiltonian of the FMOc Calculated with the FMO Method and Transition Density Approximation. After establishing variations in values of site energies and couplings due to fragmentation of BChls and the electronic coupling scheme on model systems, we proceed with computing the full electronic Hamiltonian of the FMOc. As a point of comparison for the transition-density-based FMO Hamiltonian we use a simple QM/MM model, in which electronic couplings are computed with the transition dipole approach. All calculations are performed on the monomer model represented in Figure 1 a.

Electronic Hamiltonians corresponding to different models are provided in the Supporting Information. The highest couplings in these Hamiltonians are observed for pairs of the nearest neighbors, namely BChls 1-2, 3-4, 4-5, and 5-6. Thus, we expect couplings between neighboring BChls are the most sensitive to a choice of the model, and we analyze those in detail in the following. Excitation energies and electronic couplings between neighboring BChls computed with the FMO and QM/MM methods for the FMOc are shown in Figure 6a and Figure 6b, respectively. It should be noted that TDDFT regions here differ between the models. Namely,

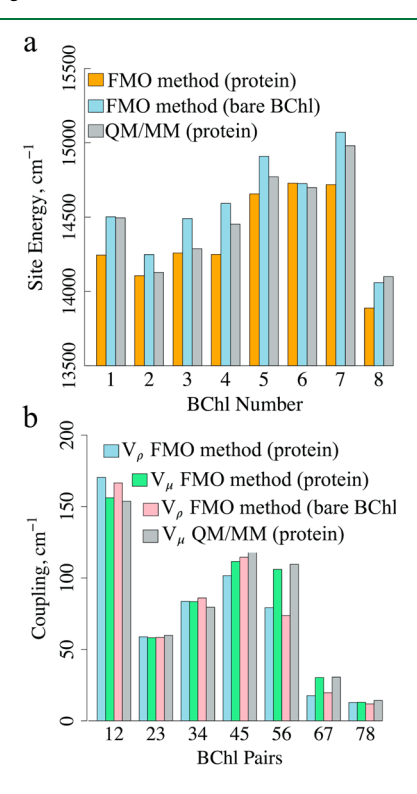


**Figure 6.** (a) Excitation energies and (b) electronic couplings in the FMOc with and without protein environment (protein and bare BChl models, respectively) computed with the FMO and QM/MM methods using transition dipole and transition density approximations.

TDDFT regions in the FMO calculations on the protein include BChls and their Mg-coordinating residues, while only BChls constitute the TDDFT part in the bare BChl model and in QM/MM.

As could be seen from Figure 6a, the protein environment affects drastically the excitation energies of BChls. For example, the difference between site energies in BChl 7 computed with the FMO method with and without protein scaffold is 352 cm<sup>-1</sup>. The differences in site energies between the FMO and QM/MM treatments are also very large, e.g., 237 cm<sup>-1</sup> in BChl 4 and 216 cm<sup>-1</sup> in BChl 6, suggesting that polarizable quantum mechanical embedding provides significant changes in excitation energies even in the case of  $\pi \to \pi^*$  transitions. However, as Figure 6b demonstrates, electronic couplings from the bare BChl and protein models differ only by 13 cm<sup>-1</sup> at most (in pair of BChl 3-4), suggesting that the protein environment influences excitation energies more substantially than electronic couplings (at least in the considered model that does not account for screening of the couplings by polarizable environment). The differences between the transition dipole and transition density approaches ( $V_o$  FMO and  $V_u$  FMO) reach 27 cm<sup>-1</sup> for BChl pairs 5-6. On the other hand, the differences in transition dipole couplings between the FMO and QM/MM models do not exceed 10 cm<sup>-1</sup> for all BChl pairs. However, it should be noted that observed deviations in couplings and site energies are a combined effect of differences in describing the protein environment and nonequivalent TDDFT regions in QM/MM and FMO models. Overall, we conclude that both quantum-mechanical polarizable embedding and transition density approach are essential for building accurate electronic Hamiltonian.

Comparison of electronic Hamiltonians computed with FMO and QM/MM methods is shown in Table 2. These Hamiltonians are produced at a single snapshot (Conformer 1) of the MD trajectory.

Table 2. Differences between Electronic Hamiltonians Obtained with Transition Density Approach in the FMO Method and with the Transition Dipole QM/MM Calculations  $(\Delta_{ij} = H_{ij}^{\text{FMO}} - H_{ij}^{\text{QM/MM}})^a$ 

| pigment | 1     | 2     | 3    | 4    | 5     | 6     | 7     | 8    |
|---------|-------|-------|------|------|-------|-------|-------|------|
| 1       | -202  | -12.8 | -1.0 | 0.5  | -0.9  | -0.8  | 7.0   | -0.2 |
| 2       | -12.8 | -58   | -1.6 | -0.7 | 0.8   | -0.4  | 6.0   | -0.1 |
| 3       | -1.0  | -1.6  | -100 | -2.7 | 5.0   | 3.2   | -9.8  | -0.3 |
| 4       | 0.5   | -0.7  | -2.7 | -237 | 18.3  | 2.5   | 30.2  | 1.1  |
| 5       | -0.9  | 0.8   | 5.0  | 18.3 | -180  | -31.8 | 16.4  | -1.9 |
| 6       | -0.8  | -0.4  | 3.2  | 2.5  | -31.8 | -216  | -20.7 | -1.6 |
| 7       | 7.0   | 6.0   | -9.8 | 30.2 | 16.4  | -20.7 | -156  | 1.8  |
| 8       | -0.2  | -0.1  | -0.3 | 1.1  | -1.9  | -1.6  | 1.8   | -23  |
|         |       |       |      |      |       |       |       |      |

<sup>&</sup>lt;sup>a</sup>The diagonal elements represent differences in site energies, while the off-diagonal elements represent differences in electronic couplings. All values are in units of cm<sup>-1</sup>.

As could be seen from Table 2, utilization of the FMO

sition density approach substantially and ts the site energies and electronic coupling pdfelement values of the differences in the Hamiltonian nto perspective, the thermal broadening proximately 200 cm<sup>-1</sup> at room temperature at 70 K, at which both absorption and CD

spectra are well resolved experimentally. Therefore, matrix elements with deviations larger than ~50 cm<sup>-1</sup> are expected to

produce noticeable differences in both absorption and CD spectra. Figure 7 visualizes absorption and CD spectra

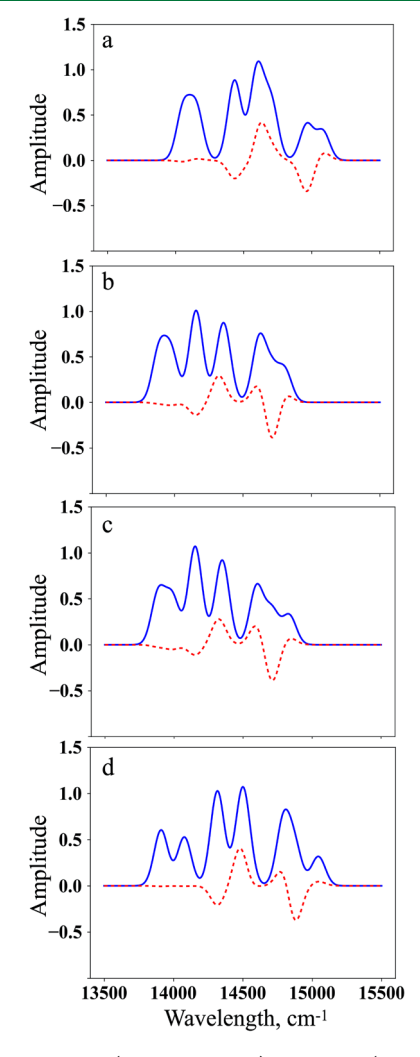
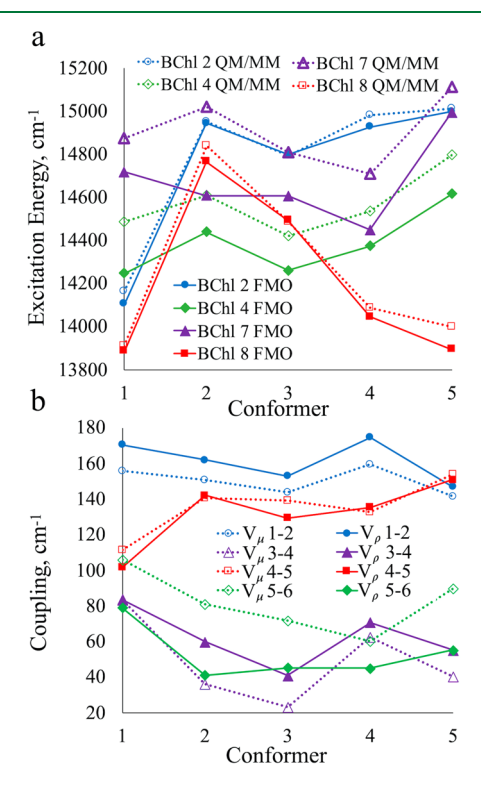


Figure 7. Absorption (blue solid line) and CD (red dashed line) spectra for various FMOc models, methods, and approximations. a) Bare BChl model computed with the FMO method and transition density approximation, b) full FMOc computed with the FMO method and transition density approximation, c) full FMOc computed with the FMO method and transition dipole approximation, and d) full FMOc computed with QM/MM and transition dipole approximation.

calculated based on four different Hamiltonians: the bare BChl model computed with the FMO method and transition density approximation (Figure 7a) and the FMOc protein model computed with the FMO method and transition density approximation (Figure 7b), with FMO and transition dipole approximation (Figure 7c), and with QM/MM and transition dipole approximation (Figure 7d). Thus, Figure 7 provides a comprehensive comparison between methods, approximations, and models of FMOc used in this study.

As could be seen from Figure 7a-d, the treatment of both the protein environment and the electronic couplings affects the calculated spectra. The transition from bare BChl to the full protein model (compare Figures 7a and 7b) substantially changes magnitudes and positions of absorption and CD spectra peaks in the entire spectroscopic region. The shift from QM/MM to FMO treatment of the protein environment (Figures 7d and 7c, respectively) results in narrowing the total width of the excitonic band, while a switch from the transition dipole to transition density approximation (Figures 7c and 7b) causes only a small effect on the spectra.

Figure 8 compares excitation energies and electronic couplings of selected pigments computed with FMO and



**Figure 8.** (a) Comparison of excitation energies computed with FMO and QM/MM and (b) comparison of density  $(\rho)$  and dipole  $(\mu)$  based couplings computed with FMO and QM/MM, respectively, both performed for 5 representative conformer structures from MD simulations.

QM/MM models at five different structural snapshots (conformers 1–5), out of which conformer 1 is the one that was used for the majority of calculations in this paper. Excitation energies and couplings for other BChls are shown in Figure S6 of the Supporting Information.

As could be seen from Figure 8a, deviations between the excitation energies with FMO and QM/MM methods are pronounced along the MD trajectory. Interestingly, for some pigments, e.g., BChl 7, the differences in site energies between FMO and QM/MM fluctuate between different snapshots, while they remain almost constant for other pigments, e.g., BChls 2, 4, and 8. The differences in couplings computed with transition dipole and transition density models also fluctuate between structural snapshots, but when the two models strongly deviate (e.g., couplings in a pair of BChls 5 and 6), this deviation is preserved along the MD trajectory. As is clear

both excitation energies and electronic fluctuate between structures, suggesting for thermal fluctuations of the protein sential for predicting accurate electronic troscopic signatures in FMOc. Thus, while y we showed how different descriptions of

the pigment-protein interactions and electronic coupling models can affect the electronic Hamiltonian and resulting spectra, we leave the questions of ensemble sampling and electron-phonon interactions to future investigation.

# V. CONCLUSIONS

We developed the computational chemistry code for treatment of electronic couplings within the FMO method and investigated how the utilization of the fully quantum mechanical description of the protein environment and transition density approximation affects the accuracy of electronic Hamiltonian of the FMOc. The all-electronic description accounts for self-consistent polarization of the environment that is overlooked with the standard nonpolarizable QM/MM description, while the utilization of transition density approximation captures fine-tuned variations of the electronic coupling. The transition from the QM/MM description to the FMO description of the protein affects the values of site energies and electronic couplings by hundreds and tens of cm<sup>-1</sup>, respectively. Analysis of model dimer systems and calculations on the whole protein suggests that the transition dipole approximation tends to overestimate the electronic coupling between BChls, but the discrepancies depend on the relative orientation of pigments and cannot be predicted a priori.

Accurate calculations with the FMO method and transition density approximation require proper fragmentation of the system, which is achieved through finding the balance between the computational cost and inclusion of functional groups involved in electronic excitations. We find that inclusion of phytol tails and an Mg-coordinating AA residue into a single BChl fragment critically improves the accuracy of the description of excitation energies and electronic couplings within the FMO method. Additionally, the pairwise combination of the charged fragments separated by not more than 5 Å improves the convergence of the self-consistent monomer cycle of FMO calculations.

We demonstrated that the description of the polarizability of the protein environment as well as the approximation utilized for calculation of the electronic couplings qualitatively affect the shape of modeled absorption and CD spectra in FMOc. Thus, development of a rigorous quantum mechanical approach is essential for predicting accurate Hamiltonians, optical spectra, and energy transfer pathways in PPCs. In the present work we demonstrated such a possibility by extending the FMO method to computing excitation energies and excitonic interactions in a multichromophore system within a single calculation. While being all-electron in nature, the FMO method cuts the computational cost by fragmenting the system and recovering critical interactions within the system by embedding each fragment into a polarizable Coulomb bath of other fragments and introducing excitonic couplings between photoactive fragments. Thus, this development provides users of the free electronic structure package GAMESS with an efficient tool for investigating excitonic interactions and FRET in a variety of molecular systems, such as natural and artificial PPCs, organic molecular crystals, and biomimetic devices.

# ASSOCIATED CONTENT

## **S** Supporting Information

The Supporting Information is available free of charge at https://pubs.acs.org/doi/10.1021/acs.jctc.9b00621.

Illustration of positive direction of transition dipole vector defined for BChl, model of BChl containing only bacteriochlorin part of pigment, models of BChls with residues in direct proximity to Mg atoms, fragmentation of BChls in bare BChl model, electronic Hamiltonian for bare BChl model calculated with FMO method and fragmentation scheme with exclusion of phytol tails, electronic Hamiltonian for bare BChl model calculated with FMO method and fragmentation scheme with inclusion of phytol tails, absorption and CD spectra for bare BChl model calculated with FMO method and fragmentation scheme with inclusion and exclusion of phytol tails, electronic Hamiltonian for full FMOc monomer model calculated with FMO method and transition density approximation, electronic Hamiltonian obtained with transition dipole approach and QM/MM method for full FMOc monomer model, excitation energies of BChls 1, 3, 5, and 6 and electronic couplings for BChl pairs 2-3, 6-7, and 7-8 at five different structural snapshots, list of negatively and positively charged fragments combined pairwise in FMO method calculations, and atomic Cartesian coordinates of BChl model containing only bacteriochlorin part of pigment (PDF)

## AUTHOR INFORMATION

## **Corresponding Author**

\*Phone: +1(765)-494-5255. E-mail: lslipchenko@purdue.edu.

ORCID ®

Danil S. Kaliakin: 0000-0002-9354-8248 Dmitri G. Fedorov: 0000-0003-2530-5989 Lyudmila V. Slipchenko: 0000-0002-0445-2990

Notes

The authors declare no competing financial interest.

#### ACKNOWLEDGMENTS

D.G.F. thanks Prof. Thomas Renger for elucidating the phase aspects for transition dipoles. D.S.K., Y.K., Q.C., and L.V.S. acknowledge support from the National Science Foundation (Grants CHE-1465154, CHE-1450088, and CHE-1800505) and from the Department of Energy, Office of Basic Energy Sciences (Grant DE-SC0018239). Q.C. was supported by the Purdue University Summer Undergraduate Research Fellowship Program. This research was supported in part through computational resources provided by Information Technology at Purdue, West Lafayette, IN.

# **■** REFERENCES

- (1) Zhou, H.; Xu, J.; Liu, X.; Zhang, H.; Wang, D.; Chen, Z.; Zhang, D.; Fan, T. Bio-Inspired Photonic Materials: Prototypes and Structural Effect Designs for Applications in Solar Energy Manipulation. *Adv. Funct. Mater.* **2018**, 28, 1705309.
- (2) Schlau-Cohen, G. S. Principles of Light Harvesting from Single Photosynthetic Complexes. *Interface Focus* **2015**, *5*, 20140088.
- (3) Llansola-Portoles, M. J.; Gust, D.; Moore, T. A.; Moore, A. L. Artificial Photographetic Antennas and Reaction Centers. C. R. Chim.



voderezhkin, V. I.; Van Grondelle, R. Quantum hesis for Bio-Inspired Solar-Energy Conversion. 55–365.

dner, R.; Köhler, J.; Lambert, C.; Würthner, F. Molecular Aggregates — From Natural Antennas

to Synthetic Chromophore Systems. Adv. Energy Mater. 2017, 7, 1700236.

- (6) Fenna, R. E.; Matthews, B. W. Chlorophyll Arrangement in a Bacteriochlorophyll Protein from Chlorobium Limicola. *Nature* **1975**, 258, 573–577.
- (7) Olson, J. M.; Cole, P.; Cox, R.; Fenna, R.; Filmer, D.; Ke, B.; Melkozernov, A.; Miller, M.; Pearlstein, R.; Raymond, J. The FMO Protein. *Photosynth. Res.* **2004**, *80*, 181–187.
- (8) Mirkovic, T.; Ostroumov, E. E.; Anna, J. M.; Van Grondelle, R.; Govindjee; Scholes, G. D. Light Absorption and Energy Transfer in the Antenna Complexes of Photosynthetic Organisms. *Chem. Rev.* **2017**, *117*, 249–293.
- (9) Huijser, A.; Marek, P. L.; Savenije, T. J.; Siebbeles, L. D. A.; Scherer, T.; Hauschild, R.; Szmytkowski, J.; Kalt, H.; Hahn, H.; Balaban, T. S. Photosensitization of TiO<sub>2</sub> and SnO<sub>2</sub> by Artificial Self-Assembling Mimics of the Natural Chlorosomal Bacteriochlorophylls. *J. Phys. Chem. C* **2007**, *111*, 11726–11733.
- (10) Vulto, S. I. E.; de Baat, M. A.; Louwe, R. J. W.; Permentier, H. P.; Neef, T.; Miller, M.; van Amerongen, H.; Aartsma, T. J. Exciton Simulations of Optical Spectra of the FMO Complex from the Green Sulfur Bacterium Chlorobium Tepidum at 6 K. J. Phys. Chem. B 1998, 102, 9577–9582.
- (11) Savikhin, S.; Buck, D. R.; Struve, W. S. Oscillating Anisotropies in a Bacteriochlorophyll Protein: Evidence for Quantum Beating between Exciton Levels. *Chem. Phys.* **1997**, 223, 303–312.
- (12) Saer, R. G.; Stadnytskyi, V.; Magdaong, N. C.; Goodson, C.; Savikhin, S.; Blankenship, R. E. Probing the Excitonic Landscape of the Chlorobaculum Tepidum Fenna-Matthews-Olson (FMO) Complex: A Mutagenesis Approach. *Biochim. Biophys. Acta, Bioenerg.* **2017**, 1858, 288–296.
- (13) Savikhin, S.; Buck, D. R.; Struve, W. S. Pump-Probe Anisotropies of Fenna-Matthews-Olson Protein Trimers from Chlorobium Tepidum: A Diagnostic for Exciton Localization? *Biophys. J.* 1997, 73, 2090–2096.
- (14) Kihara, S.; Hartzler, D. A.; Orf, G. S.; Blankenship, R. E.; Savikhin, S. The Fate of the Triplet Excitations in the Fenna-Matthews-Olson Complex. J. Phys. Chem. B 2015, 119, 5765–5772.
- (15) Buck, D. R.; Savikhin, S.; Struve, W. S. Effect of Diagonal Energy Disorder on Circular Dichroism Spectra of Fenna-Matthews-Olson Trimers. *J. Phys. Chem. B* **1997**, *101*, 8395–8397.
- (16) Nielsen, J. T.; Kulminskaya, N. V.; Bjerring, M.; Linnanto, J. M.; Rätsep, M.; Pedersen, M. Ø.; Lambrev, P. H.; Dorogi, M.; Garab, G.; Thomsen, K.; et al. In Situ High-Resolution Structure of the Baseplate Antenna Complex in Chlorobaculum Tepidum. *Nat. Commun.* **2016**, *7*, 12454.
- (17) Bína, D.; Gardian, Z.; Vácha, F.; Litvín, R. Native FMO-Reaction Center Supercomplex in Green Sulfur Bacteria: An Electron Microscopy Study. *Photosynth. Res.* **2016**, *128*, 93–102.
- (18) Thyrhaug, E.; Žídek, K.; Dostál, J.; Bína, D.; Zigmantas, D. Exciton Structure and Energy Transfer in the Fenna-Matthews-Olson Complex. J. Phys. Chem. Lett. 2016, 7, 1653–1660.
- (19) Wen, J.; Zhang, H.; Gross, M. L.; Blankenship, R. E. Membrane Orientation of the FMO Antenna Protein from Chlorobaculum Tepidum as Determined by Mass Spectrometry-Based Footprinting. *Proc. Natl. Acad. Sci. U. S. A.* **2009**, *106*, 6134–6139.
- (20) Saer, R.; Orf, G. S.; Lu, X.; Zhang, H.; Cuneo, M. J.; Myles, D. A. A.; Blankenship, R. E. Perturbation of Bacteriochlorophyll Molecules in Fenna-Matthews-Olson Protein Complexes through Mutagenesis of Cysteine Residues. *Biochim. Biophys. Acta, Bioenerg.* 2016, 1857, 1455–1463.
- (21) He, G.; Zhang, H.; King, J. D.; Blankenship, R. E. Structural Analysis of the Homodimeric Reaction Center Complex from the Photosynthetic Green Sulfur Bacterium Chlorobaculum Tepidum. *Biochemistry* **2014**, *53*, 4924–4930.
- (22) Wen, J.; Zhang, H.; Gross, M. L.; Blankenship, R. E. Native Electrospray Mass Spectrometry Reveals the Nature and Stoichiometry of Pigments in the FMO Photosynthetic Antenna Protein. *Biochemistry* **2011**, *50*, 3502–3511.
- (23) Curutchet, C.; Mennucci, B. Quantum Chemical Studies of Light Harvesting. Chem. Rev. 2017, 117, 294-343.

- (24) Chen, G. Y.; Lambert, N.; Li, C. M.; Chen, Y. N.; Nori, F. Rerouting Excitation Transfers in the Fenna-Matthews-Olson Complex. Phys. Rev. E - Stat. Nonlinear, Soft Matter Phys. 2013, 88,
- (25) Schmidt Am Busch, M.; Müh, F.; El-Amine Madjet, M.; Renger, T. The Eighth Bacteriochlorophyll Completes the Excitation Energy Funnel in the FMO Protein. J. Phys. Chem. Lett. 2011, 2, 93-
- (26) Kramer, T.; Rodriguez, M. Two-Dimensional Electronic Spectra of the Photosynthetic Apparatus of Green Sulfur Bacteria. Sci. Rep. 2017, 7, 45245.
- (27) Jia, X.; Mei, Y.; John, Z. H. Z.; Mo, Y. Hybrid QM/MM Study of FMO Complex with Polarized Protein- Specific Charge. Sci. Rep. 2015, 5, 17096.
- (28) Schuler, B.; Soranno, A.; Hofmann, H.; Nettels, D. Single-Molecule FRET Spectroscopy and the Polymer Physics of Unfolded and Intrinsically Disordered Proteins. Annu. Rev. Biophys. 2016, 45, 207-231.
- (29) Valero, J.; Pal, N.; Dhakal, S.; Walter, N. G.; Famulok, M. A Bio-Hybrid DNA Rotor-Stator Nanoengine That Moves along Predefined Tracks. Nat. Nanotechnol. 2018, 13, 496-503.
- (30) Krainer, G.; Hartmann, A.; Schlierf, M. FarFRET: Extending the Range in Single-Molecule FRET Experiments beyond 10 Nm. Nano Lett. 2015, 15, 5826-5829.
- (31) Bonilla, J. C.; Bozkurt, F.; Ansari, S.; Sozer, N.; Kokini, J. L. Applications of Quantum Dots in Food Science and Biology. Trends Food Sci. Technol. 2016, 53, 75-89.
- (32) Auer, A.; Strauss, M. T.; Schlichthaerle, T.; Jungmann, R. Fast, Background-Free DNA-PAINT Imaging Using FRET-Based Probes. Nano Lett. 2017, 17, 6428-6434.
- (33) Deußner-Helfmann, N. S.; Auer, A.; Strauss, M. T.; Malkusch, S.; Dietz, M. S.; Barth, H. D.; Jungmann, R.; Heilemann, M. Correlative Single-Molecule FRET and DNA-PAINT Imaging. Nano Lett. 2018, 18, 4626-4630.
- (34) Jiang, S.; Zhang, Y. Upconversion Nanoparticle-Based FRET System for Study of SiRNA in Live Cells. Langmuir 2010, 26, 6689-6694.
- (35) Hodgson, L.; Chan, E. W. L.; Hahn, K. M.; Yousaf, M. N. Combining Surface Chemistry with a FRET-Based Biosensor to Study the Dynamics of RhoA GTPase Activation in Cells on Patterned Substrates. J. Am. Chem. Soc. 2007, 129, 9264-9265.
- (36) Yun, C. S.; Javier, A.; Jennings, T.; Fisher, M.; Hira, S.; Peterson, S.; Hopkins, B.; Reich, N. O.; Strouse, G. F. Nanometal Surface Energy Transfer in Optical Rulers, Breaking the FRET Barrier. J. Am. Chem. Soc. 2005, 127, 3115-3119.
- (37) Dinh, T.; Renger, T. Towards an Exact Theory of Linear Absorbance and Circular Dichroism of Pigment- Protein Complexes: Importance of Non-Secular Contributions. J. Chem. Phys. 2015, 142, 034104.
- (38) Thyrhaug, E.; Zidek, K.; Dostal, J.; Bina, D.; Zigmantas, D. Exciton Structure and Energy Transfer in the Fenna-Matthews-Olson Complex. J. Phys. Chem. Lett. 2016, 7, 1653-1660.
- (39) Olbrich, C.; Jansen, T. L. C.; Liebers, J.; Aghtar, M.; Strümpfer, J.; Schulten, K.; Knoester, J.; Kleinekathöfer, U. From Atomistic Modeling to Excitation Transfer and Two-Dimensional Spectra of the FMO Light-Harvesting Complex. J. Phys. Chem. B 2011, 115, 8609-8621.
- (40) Jurinovich, S.; Curutchet, C.; Mennucci, B. The Fenna-Matthews-Olson Protein Revisited: A Fully Polarizable (TD)DFT/

pdfelement

emPhysChem **2014**, 15, 3194–3204.

rutchet, C.; Knecht, S.; Mennucci, B.; Kongsted, Prediction of the Energy Ladder in Multins: A Benchmark Study on the FMO Light-J. Chem. Theory Comput. 2013, 9, 4928-4938. 7.-J.; Ye, J.; Wang, X.; Hirao, H.; Zhao, Y. QM/

MM Modeling of Environmental Effects on Electronic Transitions of the FMO Complex. J. Phys. Chem. B 2013, 117, 3488-3495.

- (43) Adolphs, J.; Müh, F.; Madjet, M. E. A.; Renger, T. Calculation of Pigment Transition Energies in the FMO Protein: From Simplicity to Complexity and Back. Photosynth. Res. 2008, 95, 197-209.
- (44) Higashi, M.; Saito, S. Quantitative Evaluation of Site Energies and Their Fluctuations of Pigments in the Fenna-Matthews-Olson Complex with an Efficient Method for Generating a Potential Energy Surface. J. Chem. Theory Comput. 2016, 12, 4128-4137.
- (45) Chandrasekaran, S.; Aghtar, M.; Valleau, S.; Aspuru-Guzik, A.; Kleinekathöfer, U. Influence of Force Fields and Quantum Chemistry Approach on Spectral Densities of BChl a in Solution and in FMO Proteins. J. Phys. Chem. B 2015, 119, 9995-10004.
- (46) You, Z.-Q.; Hsu, C.-P. Theory and Calculation for the Electronic Coupling in Excitation Energy Transfer. Int. J. Quantum Chem. 2014, 114, 102-115.
- (47) Gordon, M. S.; Fedorov, D. G.; Pruitt, S. R.; Slipchenko, L. V. Fragmentation Methods: A Route to Accurate Calculations on Large Systems. Chem. Rev. 2012, 112, 632-672.
- (48) Fedorov, D. G. The Fragment Molecular Orbital Method: Theoretical Development, Implementation in GAMESS, and Applications. Wiley Interdiscip. Rev. Comput. Mol. Sci. 2017, 7, e1322.
- (49) Hestand, N. J.; Tempelaar, R.; Knoester, J.; Jansen, T. L. C.; Spano, F. C. Exciton Mobility Control through Sub-A Packing Modifications in Molecular Crystals. Phys. Rev. B: Condens. Matter Mater. Phys. 2015, 91, 195315.
- (50) Yamagata, H.; Pochas, C. M.; Spano, F. C. Designing J- and H -Aggregates through Wave Function Overlap Engineering: Applications to Poly (3-Hexylthiophene). J. Phys. Chem. B 2012, 116, 14494-14503.
- (51) Hestand, N. J.; Spano, F. C. Interference between Coulombic and CT-Mediated Couplings in Molecular Aggregates: H- to J-Aggregate Transformation in Perylene-Based  $\pi$ -Stacks. J. Chem. Phys. 2015, 143, 244707.
- (52) Andrews, D. L.; Curutchet, C.; Scholes, G. D. Resonance Energy Transfer: Beyond the Limits. Laser Photonics Rev. 2011, 5, 114-123.
- (53) Cupellini, L.; Corbella, M.; Mennucci, B.; Curutchet, C. Electronic Energy Transfer in Biomacromolecules. WIREs Comput. Mol. Sci. 2019, 9, e1392.
- (54) Hestand, N. J.; Kazantsev, R. V.; Weingarten, A. S.; Palmer, L. C.; Stupp, S. I.; Spano, F. C. Extended-Charge-Transfer Excitons in Crystalline Supramolecular Photocatalytic Sca Ffolds. J. Am. Chem. Soc. 2016, 138, 11762-11774.
- (55) Fornari, R. P.; Rowe, P.; Padula, D.; Troisi, A. Importance and Nature of Short-Range Excitonic Interactions in Light Harvesting Complexes and Organic Semiconductors. J. Chem. Theory Comput. 2017, 13, 3754-3763.
- (56) Pettersson, K.; Kyrychenko, A.; Ro, E.; Ljungdahl, T. Singlet Energy Transfer in Porphyrin-Based Donor-Bridge -Acceptor Systems: Interaction between Bridge Length and Bridge Energy. J. Phys. Chem. A 2006, 110, 310-318.
- (57) Hestand, N. J.; Spano, F. C. Determining the Spatial Coherence of Excitons from the Photoluminescence Spectrum in Charge-Transfer J-Aggregates. Chem. Phys. 2016, 481, 262-271.
- (58) Hsu, C. P.; You, Z. Q.; Chen, H. C. Characterization of the Short-Range Couplings in Excitation Energy Transfer. J. Phys. Chem. C 2008, 112, 1204-1212.
- (59) Shao, Y.; Gan, Z.; Epifanovsky, E.; Gilbert, A. T. B.; Wormit, M.; Kussmann, J.; Lange, A. W.; Behn, A.; Deng, J.; Feng, X.; et al. Advances in Molecular Quantum Chemistry Contained in the Q-Chem 4 Program Package. Mol. Phys. 2015, 113, 184-215.
- (60) Tanaka, S.; Mochizuki, Y.; Komeiji, Y.; Okiyama, Y.; Fukuzawa, K. Electron-Correlated Fragment-Molecular-Orbital Calculations for Biomolecular and Nano Systems. Phys. Chem. Chem. Phys. 2014, 16, 10310-10344.
- (61) Nakano, T.; Kaminuma, T.; Sato, T.; Akiyama, Y.; Uebayasi, M.; Kitaura, K. Fragment Molecular Orbital Method: Application to Polypeptides. Chem. Phys. Lett. 2000, 318, 614-618.

- (62) Fedorov, D. G.; Kitaura, K. The Importance of Three-Body Terms in the Fragment Molecular Orbital Method. *J. Chem. Phys.* **2004**, *120*, 6832–6840.
- (63) Ishikawa, T.; Ishikura, T.; Kuwata, K. Theoretical Study of the Prion Protein Based on the Fragment Molecular Orbital Method. *J. Comput. Chem.* **2009**, *30*, 2594–2601.
- (64) Takami, T.; Maki, J.; Ooba, J.; Inadomi, Y.; Honda, H.; Susukita, R.; Inoue, K.; Kobayashi, T.; Nogita, R.; Aoyagi, M. Multi-Physics Extension of OpenFMO Framework. *AIP Conf. Proc.* **2007**, 963, 122–125.
- (65) Fujita, T.; Mochizuki, Y. Development of the Fragment Molecular Orbital Method for Calculating Nonlocal Excitations in Large Molecular Systems. *J. Phys. Chem. A* **2018**, *122*, 3886–3898.
- (66) Polyakov, I. V.; Khrenova, M. G.; Moskovsky, A. A.; Shabanov, B. M.; Nemukhin, A. V. Towards First-Principles Calculation of Electronic Excitations in the Ring of the Protein-Bound Bacteriochlorophylls. *Chem. Phys.* **2018**, *505*, 34–39.
- (67) Nakata, H.; Fedorov, D. G.; Yokojima, S.; Kitaura, K.; Sakurai, M.; Nakamura, S. Unrestricted Density Functional Theory Based on the Fragment Molecular Orbital Method for the Ground and Excited State Calculations of Large Systems. *J. Chem. Phys.* **2014**, *140*, 144101.
- (68) Fedorov, D. G.; Kitaura, K. Multiconfiguration Self-Consistent-Field Theory Based upon the Fragment Molecular Orbital Method. *J. Chem. Phys.* **2005**, *122*, No. 054108.
- (69) Fedorov, D. G.; Kitaura, K. Second Order Møller-Plesset Perturbation Theory Based upon the Fragment Molecular Orbital Method. *J. Chem. Phys.* **2004**, *121*, 2483–2490.
- (70) Fedorov, D. G.; Kitaura, K. Coupled-Cluster Theory Based upon the Fragment Molecular-Orbital Method. *J. Chem. Phys.* **2005**, 123, 134103.
- (71) Chiba, M.; Fedorov, D. G.; Kitaura, K. Time-Dependent Density Functional Theory Based upon the Fragment Molecular Orbital Method. *J. Chem. Phys.* **2007**, *127*, 104108.
- (72) Alexeev, Y.; Mahajan, A.; Leyffer, S.; Fletcher, G.; Fedorov, D. G. Heuristic Static Load-Balancing Algorithm Applied to the Fragment Molecular Orbital Method. In SC International Conference for High Performance Computing, Networking, Storage and Analysis; Salt Lake City. Utah. USA. 2012; DOI: 10.1109/SC.2012.62.
- (73) Takeda, R.; Kobayashi, I.; Suzuki, R.; Kawai, K.; Kittaka, A.; Takimoto-Kamimura, M.; Kurita, N. Proposal of Potent Inhibitors for Vitamin-D Receptor Based on Ab Initio Fragment Molecular Orbital Calculations. *J. Mol. Graphics Modell.* **2018**, *80*, 320–326.
- (74) Choi, J.; Kim, H.-J.; Jin, X.; Lim, H.; Kim, S.; Roh, I.-S.; Kang, H.-E.; No, K. T.; Sohn, H.-J. Application of the Fragment Molecular Orbital Method to Discover Novel Natural Products for Prion Disease. Sci. Rep. 2018, 8, 13063.
- (75) Ishikawa, T.; Mizuta, S.; Kaneko, O.; Yahata, K. Fragment Molecular Orbital Study of the Interaction between Sarco/Endoplasmic Reticulum Ca<sup>2+</sup>-ATPase and Its Inhibitor Thapsigargin toward Anti-Malarial Development. *J. Phys. Chem. B* **2018**, *122*, 7970–7977.
- (76) Pruitt, S. R.; Steinmann, C. Mapping Interaction Energies in Chorismate Mutase with the Fragment Molecular Orbital Method. *J. Phys. Chem. A* **2017**, *121*, 1797–1807.
- (77) Chiba, M.; Fedorov, D. G.; Kitaura, K. Time-Dependent Density Functional Theory with the Multilayer Fragment Molecular Orbital Method. *Chem. Phys. Lett.* **2007**, 444, 346–350.
- (78) Schmidt, M. W.; Baldridge, K. K.; Boatz, J. A.; Elbert, S. T.;

pdfelement

- n, J. H.; Koseki, S.; Matsunaga, N.; Nguyen, K. neral Atomic and Molecular Electronic Structure *hem.* **1993**, *14*, 1347–1363.
- S.; Schmidt, M. W. Advances in Electronic GAMESS a Decade Later. In *Theory and* putational Chemistry; Dykstra, C. E.; Frenking,
- G.; Kim, K. S.; Scuseria, G. E., Eds.; Elsevier: Amsterdam, 2005; pp 1167–1189, DOI: 10.1016/B978-044451719-7/50084-6.

- (80) Hsu, C. P.; Fleming, G. R.; Head-Gordon, M.; Head-Gordon, T. Excitation Energy Transfer in Condensed Media. *J. Chem. Phys.* **2001**, *114*, 3065–3072.
- (81) Curutchet, C.; Muñoz-Losa, A.; Monti, S.; Kongsted, J.; Scholes, G. D.; Mennucci, B. Electronic Energy Transfer in Condensed Phase Studied by a Polarizable QM/MM Model. *J. Chem. Theory Comput.* **2009**, *5*, 1838–1848.
- (82) Olsen, J. M.; Aidas, K.; Kongsted, J. Excited States in Solution through Polarizable Embedding. J. Chem. Theory Comput. 2010, 6, 3721–3734.
- (83) Guido, C. A.; Jacquemin, D.; Adamo, C.; Mennucci, B. Electronic Excitations in Solution: The Interplay between State Specific Approaches and a Time-Dependent Density Functional Theory Description. *J. Chem. Theory Comput.* **2015**, *11*, 5782–5790.
- (84) Ren, S.; Lipparini, F.; Mennucci, B.; Caricato, M. Coupled Cluster Theory with Induced Dipole Polarizable Embedding for Ground and Excited States. *J. Chem. Theory Comput.* **2019**, *15*, 4485–4496
- (85) Slipchenko, L. V. Solvation of the Excited States of Chromophores in Polarizable Environment: Orbital Relaxation versus Polarization. *J. Phys. Chem. A* **2010**, *114*, 8824–8830.
- (86) Garab, G.; van Amerongen, H. Linear Dichroism and Circular Dichroism in Photosynthesis Research. *Photosynth. Res.* **2009**, *101*, 135–146.
- (87) Vázquez, J. T. Features of Electronic Circular Dichroism and Tips for Its Use in Determining Absolute Configuration. *Tetrahedron: Asymmetry* **2017**, *28*, 1199–1211.
- (88) Miles, A. J.; Wallace, B. A. Circular Dichroism Spectroscopy for Protein Characterization: Biopharmaceutical Applications. In *Biophysical Characterization of Proteins in Developing Biopharmaceuticals*; Elsevier B.V.: London, UK, 2015; pp 109–137, DOI: 10.1016/B978-0-444-59573-7.00006-3.
- (89) Gattuso, H.; Assfeld, X.; Monari, A. Modeling DNA Electronic Circular Dichroism by QM/MM Methods and Frenkel Hamiltonian. *Theor. Chem. Acc.* **2015**, *134*, *36*.
- (90) Prokhorenko, V. I.; Steensgaard, D. B.; Holzwarth, A. R. Exciton Theory for Supramolecular Chlorosomal Aggregates: 1. Aggregate Size Dependence of the Linear Spectra. *Biophys. J.* **2003**, *85*, 3173–3186.
- (91) Hodecker, M.; Biczysko, M.; Dreuw, A.; Barone, V. Simulation of Vacuum UV Absorption and Electronic Circular Dichroism Spectra of Methyl Oxirane: The Role of Vibrational Effects. *J. Chem. Theory Comput.* **2016**, *12*, 2820–2833.
- (92) Case, D. A.; Darden, T.; Cheatham, T. E., III; Simmerling, C.; Brook, S.; Roitberg, A.; Wang, J.; Southwestern, U. T.; Duke, R. E.; Hill, U. *AMBER* 2014; Univ. California, San Francisco.
- (93) Tronrud, D. E.; Blankenship, A. R. E.; Gay, L. The Structural Basis for the Difference in Absorbance Spectra for the FMO Antenna Protein from Various Green Sulfur Bacteria. *Photosynth. Res.* **2009**, 100, 79–87.
- (94) Maier, J. A.; Martinez, C.; Kasavajhala, K.; Wickstrom, L.; Hauser, K. E.; Simmerling, C. Ff14SB: Improving the Accuracy of Protein Side Chain and Backbone Parameters from Ff99SB. *J. Chem. Theory Comput.* **2015**, *11*, 3696–3713.
- (95) Jorgensen, W. L.; Chandrasekhar, J.; Madura, J. D.; Impey, R. W.; Klein, M. L. Comparison of Simple Potential Functions for Simulating Liquid Water. *J. Chem. Phys.* **1983**, *79*, 926.
- (96) Wang, J.; Wolf, R. M.; Caldwell, J. W.; Kollman, P. A.; Case, D. A. Development and Testing of a General Amber Force Field. *J. Comput. Chem.* **2004**, *25*, 1157–1174.
- (97) Ceccarelli, M.; Procacci, P.; Marchi, M. An Ab Initio Force Field for the Cofactors of Bacterial Photosynthesis. *J. Comput. Chem.* **2003**, 24, 129–142.
- (98) Darden, T.; York, D.; Pedersen, L. Particle Mesh Ewald: An N-log(N) Method for Ewald Sums in Large Systems. *J. Chem. Phys.* **1993**, *98*, 10089–10092.
- (99) Essmann, U.; Perera, L.; Berkowitz, M. L.; Darden, T.; Lee, H.; Pedersen, L. G. A Smooth Particle Mesh Ewald Method. *J. Chem. Phys.* **1995**, *103*, 8577–8593.

- (100) Pettersen, E. F.; Goddard, T. D.; Huang, C. C.; Couch, G. S.; Al, E. UCSF Chimera a Visualization System for Exploratory Research and Analysis. *J. Comput. Chem.* **2004**, *25*, 1605—1612.
- (101) Ernzerhof, M.; Scuseria, G. E. Assessment of the Perdew-Burke-Ernzerhof Exchange-Correlation Functional. *J. Chem. Phys.* **1999**, *110*, 5029–5036.
- (102) Petersson, G. A.; Al-Laham, M. A. A Complete Basis Set Model Chemistry. II. Open-Shell Systems and the Total Energies of the First-Row Atoms. *J. Chem. Phys.* **1991**, *94*, 6081–6090.
- (103) Fletcher, G. D.; Fedorov, D. G.; Pruitt, S. R.; Windus, T. L.; Gordon, M. S. Large-Scale MP2 Calculations on the Blue Gene Architecture Using the Fragment Molecular Orbital Method. *J. Chem. Theory Comput.* **2012**, *8*, 75–79.

